Bioprinting 13 (2018) e00039

Contents lists available at ScienceDirect

Bioprinting

journal homepage: www.elsevier.com/locate/bprint

Large 3D bioprinted tissue: Heterogeneous perfusion and vascularization

Lea Pourchet[a], Emma Petiot[a], Céline Loubière[c], Eric Olmos[c], Morgan Dos Santos[b], Amélie Thépot[b], Blum J. Loïc[a], Christophe A. Marquette[a,*]

[a] 3d.FAB, Univ Lyon, Université Lyon1, CNRS, INSA, CPE-Lyon, ICBMS, UMR 5246, Bat. Lederer, 1 rue Victor Grignard, 69100 Villeurbanne, France
[b] LabSkin Creations, Edouard Herriot Hospital, 5 place d'Arsonval, Bâtiment 5, 69437 Lyon, France
[c] Laboratoire Réactions et Génie des Procédés, Université de Lorraine, CNRS, LRGP, F-54000 Nancy, France

ARTICLE INFO

Keywords:
3D bioprinting
Bioreactor
Computational fluid dynamics
Endothelial cells
Fibroblasts
Microvascularization

ABSTRACT

Large bioprinted tissues (dm^3) are more and more accessible but their *in vitro* culture and maturation conditions stay an unchartered territory. In the present report, we aim to present a preliminary study of endothelialized large bioprinted tissues (fibroblast and human dermal microvascular endothelial cells) maturation using silicone 3D printed perfusion system (bioreactor). Computational Fluid Dynamics (CFD) simulation was used to relate the theoretical culture medium flow path within the large bioprinted tissue with the actual tissue morphology and composition, obtained through histological observations. The obtained results demonstrate the positive impact of using dynamic maturation conditions (300 mL/h culture medium flow rate) on the extracellular matrix production and the conservation of the large bioprinted tissue internal geometry. Clear differences between static and dynamic culture conditions were herein found. Finally, typical microvascular organization, composed of human dermal microvascular endothelial cells organized around an open lumen, were found within the large bioprinted tissue.

1. Introduction

In the last 5 years, bioprinting became a highly active scientific area in which multidisciplinary expertise is the key to success [1]. Nevertheless, the expectations of the field for regenerative medicine applications, involving large living tissues (in the cm^3 to dm^3 range) were far than fulfill. Indeed, issues related to vascularization of large tissue or organ strongly impedes their *in vitro* maturation. A strong effort should be put in processes and scale-up strategies development, suitable for customized tissues' production [2]. This scale-up will have to go through specific and controlled bioreactors developments and behavior modeling. For a better understanding, defining the word "bioreactor" is essential. Martin et al. [3] defined bioreactors as devices in which biological and/or biochemical processes operate under closely monitored and tightly controlled environmental and operating conditions (*e.g.*, pH, temperature, pressure, nutrient supply, and waste removal). Conventionally, bioreactor studies may be separated into two groups: bioreactor for cell culture (either suspension or 2D adherent cells) and bioreactor for *in vitro* tissues maturation. While the first group has been exploited and studied for many years and already benefits from abundant literature, for example for virus or active biomolecule productions [4], the second one lacks adaptability, particularly when it comes to specific tissue maturation conditions (mechanical stress, perfusion) but also concerning the actual design and shape of the targeted tissue or organ. Only seldom published studies attempted to address these issues, like specific maturation bioreactors for large bone defects [5], osteochondral constructs [6], cardiac tissues [7], biomaterial sponge vascularization [8].

In one of our previous work, the achievement of 3D bioprinted fibroblast-based tissues (cm^2 full skin patches) was demonstrated [9]. Nevertheless, bioprinted tissues size and thickness were limited by the fact that these tissue were not vascularized. Consequently, the increase of these tissues' size up to the dm^3, necessitates the concomitant development of i) specific bioprinted tissue architecture and ii) dedicated perfusion system maintaining cell viability thanks to continuous medium flow and nutriment supply.

The present work took place in the general context of the culture and maturation of large bioprinted tissues, before *in situ* neo-vascularization takes place. In an attempt to bring partial solution to this problem, the present work evaluates possible efficient avenues for the production of dm^3 bioprinted tissues through: i) internal tissue geometry leading to easy culture medium perfusion and ii) design of on demand perfusion system (bioreactor) perfectly fitting the size and shape of the bioprinted tissues. Such system is expected to allow both the maturation of large bioprinted tissues in dynamic conditions and the induction of vascularization. Our secondary goal was to obtain

* Corresponding author.
E-mail address: christophe.marquette@univ-lyon1.fr (C.A. Marquette).

https://doi.org/10.1016/j.bprint.2018.e00039
Received 25 July 2018; Received in revised form 8 November 2018; Accepted 3 December 2018

macroscopic organization of the tissue thanks to the internal lattice of the 3D bioprinting together with a correct arrangement at the cellular level. In other words, a microvascularisation (cells self-organization) connected to macrovascularisation (3D printed internal structures). A complementary approach based on Computational Fluid Dynamics (CFD) simulation was used to link the theoretical culture medium flow path within the large bioprinted tissue with the actual tissue morphology and composition.

2. Materials and methods

2.1. Cells' isolation and cultivation

Foreskin samples were obtained from healthy patients undergoing circumcision according to French regulation, including declaration to ministry (DC No. 2014-2281) and procurement of written informed consent from the patient. Fibroblasts were isolated from 2 years-old donor and cultivated in flasks at 37 °C, 5% CO_2 in Dulbecco's modified Eagle medium (DMEM)/Glutamax TM-1 medium (Gibco Cell Culture, Invitrogen, France), supplemented with 10% calf bovine serum (HyClone™, GE Healthcare Life Sciences, France), 1% penicillin, streptomycin and amphotericin B (Bio Industries-Cliniscience, France). Culture medium was changed every 2 days and cells were routinely passaged in culture flasks until bioprinting. Cells of passages between 7 and 9 were used.

Human dermal microvascular endothelial cells expressing GFP were kindly supplied by Dr. Jean-Jacques Feige [10] and cultivated in the same conditions as fibroblasts.

2.2. Bioink formulation and bioprinting procedure

Bioink consisted in a mixture of 10% (w/v) bovine gelatine (Sigma-Aldrich, France), 2% (w/v) fibrinogen (Sigma-Aldrich, France) and 0.5% (w/v) very low viscosity alginate (Alpha Aesar, France) dissolved in NaCl 0.9% (Laboratoire Aguettant, France), as already described [9]. Just before printing, cells were trypsinized and seeded in the bioink, homogenized and loaded in a sterile 10 mL syringe (Nordson, USA). The syringe was then stored for 15 min at 37 °C in orderto reach appropriateprintable rheology of the ink. Bioprinting of the tissue was performed using our in-house developed bioprinter (TOBECA, France [9]), a tronconical nozzle with inner diameter of 400 µm (Nordson, USA) and our previously published optimized bioink [9]. Bioprinted large tissues were then immerged in a 0.05% (w/v) thrombin (30–400 NIH/mg, Sigma Aldrich, France) / 3% (w/v) calcium chloride (Sigma Aldrich, France) solution to polymerize fibrinogen and alginate during 1 H at room temperature.

2.3. Perfusion system 3D printing and operational conditions

The bioreactors were printed in silicone (Sikasil®-C, SIKA, Swiss) using the BioAssembly Bot 3D robotic printer (Advanced Solutions, USA) equipped with a tronconical nozzle with inner diameter of 400 µm (Nordson, USA). An additional acrylate cover, connected to a sterile filter for vent and gas exchange was printed using a commercially available inkjet printer (Objet Pro, Stratasys, France; VeroClear RGD810).

The culture within the perfusion system was performed with same cultivation medium as described previously (Section 2.1) using an inlet flowrate of 300 mL/h (Peristaltic Pump *P*-1, GE Healthcare Life Science. In order to permit temperature control and pH buffering within the bioreactor, the perfusion system was placed directly in a standard CO_2 cell culture incubator.

2.4. Histological and immunohistochemical analysis

After 7 days of maturation, large bioprinted tissues were immediately fixed in 4% formalin and embedded in paraffin. Then, paraffin-embedded formalin-fixed samples were cut into 3 µm sections. After dewaxing and rehydration, sections were stained with Masson's Trichrome (light green) for routine histology. For immunohistochemistry, labelling was performed on 5 µm sections and incubated with anti-endothelium EN4 mouse monoclonal primary antibody (ABCAM ab8087). A staining kit (ImmPRES™ excel staining kit-7602) was used as a secondary antibody and incubated for 1 h at room temperature. A nuclear counterstaining was performed using Harris Hematoxylin.

Specimens stained in Masson's Trichrome were observed using an optical microscope, and images were captured using DSU-3 camera and NIS-Elements software.

Immunohistochemistry specimens were visualized using a Nikon Eclipse Ts2R inverted microscope and images were captured using DS-Fi3 high-definition colour camera. Eight-bit images were saved in an uncompressed image file format (lsm).

2.5. Computational fluid dynamics (CFD)

CFD simulations were performed thanks to the commercial finite solver ANSYS Fluent and data post-treatment was realized with CFD-Post software (ANSYS Inc., version 16.1). The steady-state approach was used and the flow was supposed laminar. A wall boundary condition, *i.e.* zero-velocity, was applied for bioreactor boundaries and tissue zones. The mass and momentum conservation Eqs. (Eqs. (1) and (2)) were solved for the liquid phase supposing water properties at 37 °C (density $\rho = 993\ \mathrm{kg\ m^{-3}}$ and dynamic viscosity $\mu = 6.92 \times 10^{-4}\ \mathrm{Pa\ s^{-1}}$), with $\boldsymbol{v}$ is the fluid velocity, p the pressure and $\boldsymbol{g}$ the acceleration due to gravity.

$$\nabla\bullet(\rho\boldsymbol{v}) = 0 \quad (1)$$

$$\nabla\bullet(\rho\boldsymbol{v}\boldsymbol{v}) = -\nabla p - \nabla\bullet\bar{\bar{\boldsymbol{\tau}}} + \rho\boldsymbol{g} \quad (2)$$

The calculation mesh consisted in approximately 19 million of tetrahedral meshes. Pressure-velocity coupling was solved using a SIMPLE method and pressure and momentum transport equations were discretized using 2nd order UPWIND schemes. Convergence of the simulations was verified by monitoring liquid velocities till complete stabilization.

3. Results

3.1. System architecture and design

Taking full advantage of the latest developments in 3D printing, the proposed approach consists in producing both the perfusion system (bioreactor) and the living tissue using additive manufacturing techniques. The bioreactors were indeed printed through silicone (Sikasil®-C, SIKA, Swiss) cold extrusion printing, while the tissues were printed using cold extrusion bioprinting. This approach, consisting in 3D printing both the reagent cartridge and the living tissue, has been introduced by Jennifer Lewis group in 2016. In such study a fugitive ink was used to produce hollow networks connected to a perfusion system [11]. This pioneer work was an attempt in building a vascular network of controlled shape and structure within a cm^3 living tissue. Our study is complementary to this work as the 3D bioprinting properties of our developed bioink and methods permits the direct production of tissue specifically shaped to enable perfusion.

The silicone perfusion system was designed to enable flexible inlet and outlet position of the flow thanks to choice of needle puncture in the silicone (Fig. 1-A). An additional acrylate cover, connected to a sterile filter for vent and gas exchange was printed using a commercially available inkjet printer (Objet Pro, Stratasys, France; VeroClear RGD810). Acrylate cover was extensively washed in 70% v/v ethanol/water for five days to remove any traces of toxic residues (acrylate monomers and photoinitiators) prior cell culture. The CAD file of the complete set-up can be found in an open source format at https://gist.github.com/FabricAdvancedBiology.

The large bioprinted tissue was of 8 cm^3 (2 × 2 × 2 cm) and composed of 1 million fibroblasts (normal human dermal fibroblasts from

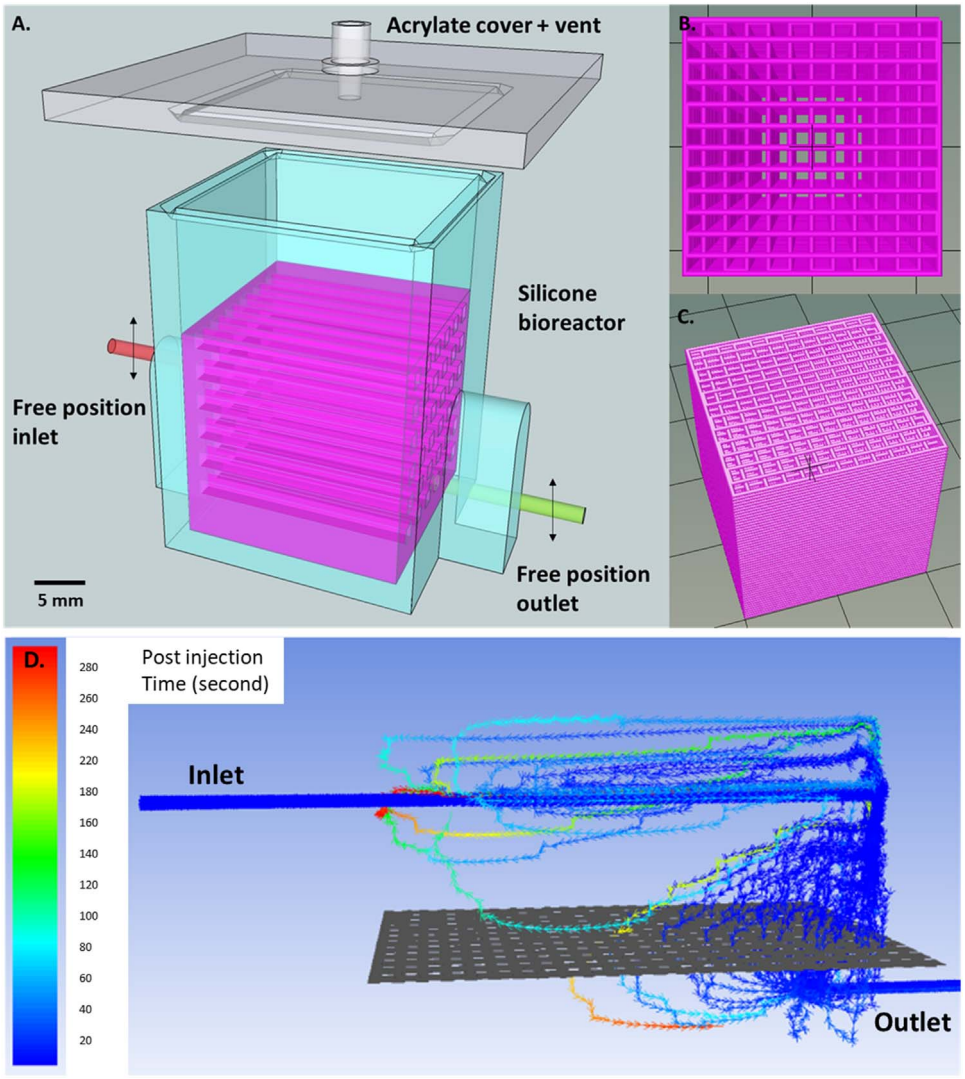

Fig. 1. A. view of the 3D printed perfusion system with its inlet and outlet free positioning (through needle puncture). B. and C. 3D view of the bioprinted large tissue showing internal macro-porosity. D. Path lines of liquid flow within the perfusion system. Colors represent post injection time, *i.e.* time necessary to a finite element to reach a particular position within the large bioprinted tissue. (For interpretation of the references to color in this figure legend, the reader is referred to the web version of this article).

young donor, 2 y.o. prepared according to Shahabeddin et al. [12]) and 5 million human dermal microvascular endothelial cells (hDMEC). Fibroblasts were herein used for their capacity to produce rapidly a well-organized extracellular matrix (ECM) network, thus consolidating the printed object. The endothelial cells were used to initiate the recapitulation of microvascular structures. The 8 cm^3 large bioprinted tissue was produced with an internal lattice leaving 80% of the object volume open to culture medium diffusion (Fig. 1-B, C**)**. This particular lattice was chosen so that the tissue thickness in every part of the objects never exceed 1 mm, while keeping the total volume of the object at 8 cm^3. This thickness was chosen according to the classically accepted passive diffusion limit of nutriment and gas of 500 µm given by Jos Malda and co-workers [13] for cartilaginous constructs. This 20% infill leads to the production of millimeters size macro-porosity within the tissue. Additionally, our printed object presents full walls on four perimeters to orientate flow in a single direction within the object. Computational Fluid Dynamics (CFD) was used to simulate the culture medium flow within the large bioprinted tissue. Fig. 1-D depicted the flow conditions and object internal shape, leading to heterogeneous fluid flow velocities and a residence time with a large distribution within the bioprinted tissue. As can be seen, a clear preferential path was created with low residency times and high velocities (see Supplementary information 1).

Such conditions were chosen as an attempt to create a 3D preferential development within the tissue. Indeed, in the present approach, we aim to use heterogeneity to generate predictable heterogeneous development in the final object, leading to localized ECM and vascularization. Three complementary simulations were realized, by multiplying the value of the inlet flow rate $Q = 300$ mL/h by a factor 0.125, 0.25 and 4. The velocity fields simulated by CFD numerical simulations provided statistic distributions of velocity, characterized by a mean velocity magnitude value µ and a standard deviation σ. The heterogeneity of the distribution of the velocity field was characterized by the coefficient of variation $C_V = \frac{\sigma}{\mu}$.

The results are provided in Table 1. Our results show that the increase of inlet flow rate entailed a clear increase of the coefficient of variation C_v and thus a relative increase of velocity heterogeneity. It is also important to note that the homogeneity observed at low flow rates were essentially the consequence of the occurrence of near-zero velocity zones (Supplementary information 2). These zones are expected to impact negatively nutrients transport and cell growth and should be thus *a priori* limited. These results also demonstrated that the increase of flow rate to higher values may question the validity of the laminar regime hypothesis ($Re < 2100$) which was made in our simulations. Thus, the use of the flow rate of 300 mL/h offered a good compromise between flow heterogeneity ($C_V = 0.48$), limitation of stagnant zones and well-established laminar regime (Re=377).

Table 1
Impact of inlet flow rate on the liquid velocity homogeneity and on Reynolds number.

Flowrate (mL/h)	Mean velocity (m/s)	Coefficient of variation C_v	Reynolds number
37.5	3.02×10^{-4}	0.07	47
75	5.89×10^{-4}	0.14	94
300	2.58×10^{-3}	0.48	377
1200	1.16×10^{-2}	1.81	1508

3.2. Large bioprinted tissue maturation

The large bioprinted tissue was cultivated for 12 days in the perfusion system using an inlet flowrate of 300 mL/h of culture medium with daily injection of vitamin C (50 µg/mL final concentration), a well-known fibroblast growth factor used to trigger extracellular matrix secretion [14]. In order to permit temperature control and pH buffering within the bioreactor, this latter was placed directly in a standard CO_2 cell culture incubator.

After one week of dynamic culture, the tissue exhibited a clear isomorphic volume reduction from 8 cm^3 to 6 cm^3, typical of the fibroblast based tissue maturation in which newly synthetized ECM and cells' attachment induces retraction [15]. This ECM production was evidenced in Fig. 2-B through Masson's Trichrome staining. Fig. 2-B also depicted the internal macro-porosity of the large bioprinted tissue. As a matter of fact, the initial millimeter size porosity was conserved during the dynamic tissue maturation, leading to tubular structures within the bioprinted tissue orientated toward the perfusion flow direction and perpendicular to the 3 µm histological section. Comparison between the heterogeneity of the obtained extracellular matrix production and the flow velocity distribution within the object showed a clear link between both phenomena (Fig. 2-B and -C). Indeed, a very low production of ECM was found in zone-A with a clear impact of the position of the needle entry. Then, zone-B, which is characterized by a wider spreading of the flow velocity, evidenced a more homogeneous ECM production. Finally, in agreement with the flow and post injection time (Fig. 1-D), zone-C depicted the most intense and homogeneous ECM production. Interestingly, this ECM production variability within the tissue was also directly related to the mechanical stress applied. Indeed, the fluid shear stress fields of zones A, B and C depicted in Fig. 2-D clearly demonstrate a direct correlation between mechanical stimulation and ECM production [16]. It is then clear that in the present system, an additive effect of localized nutrient availability and mechanical stimulation lead to localized tissue maturation.

Taking a closer look at the tissue structuration and composition using Fig. 3-A histological micrographs, the tissue was fully colonized by viable and spread cells surrounded by green staining, proof of the presence of neo-synthetized ECM and collagen secreted by the fibroblasts. It is also worth to mention that the large bioprinted tissue evidenced a strong accumulation of cells and ECM at the interface between the printed object and the culture medium. These cells were identified, using hematoxylin counterstaining and EN4 immunohistochemistry labelling, to be preferentially fibroblast at the interface (no EN4 labelling, violet staining of the nuclei), whereas human dermal microvascular endothelial cells were found to be distributed within the tissue (brown EN4 labelling) (Fig. 3-B).

The presence of the human dermal microvascular endothelial cells was also confirmed through observation of the whole bioprinted tissue with fluorescent optical microscopy (Fig. 3-C). Numerous fluorescent microstructures were found within the bioprinted large tissue with clear interconnected tubular organization. Finally, investigations were performed on the large bioprinted tissue to detect the presence of typical microvascular organization composed of human dermal microvascular endothelial cells organized around an open lumen [17]. Two examples of such organization are presented in Fig. 3-D. Thus, typical micro vessel were found with lumen inner diameters between 5 and 25 µm. These microvessels' formation in the absence of any additional growth factor was previously observed for co-culture fibroblast and endothelial cell [18]. This is also in agreement with several studies available in the scientific literature where fibroblasts were found to stabilize endothelial cell-lined tube formation [19], and provide important signaling that leads to the maturation of capillaries made of HUVEC [20,21]. Fibroblasts are known to release many growth factors including VEGF, FGF, platelet-derived growth factor (PDGF), and angiopoietin-1 [21–25].

In order to identify the impact of dynamic culture conditions on the large bioprinted tissue maturation, a control experiment was performed using an identical large bioprinted tissue matured in static culture conditions, *i.e.* without perfusion flow. First important observation is the poor conservation of the structuration and of the internal initial millimeter size porosity with only seldom remaining tubular structures (Supplementary information 3-A). Then, the typical fibroblast's tissue retraction [26] observed for the tissue cultures under dynamic conditions (retraction factor of 70%), was minimal with only a 10% retraction factor. Also, a clear lower density of extracellular matrix ECM was produced under static culture conditions with green staining only rarely dense (Supplementary information 3-B). These two observations are of course related, considering that *in vivo*, different proteins secreted by fibroblasts progressively accumulate and already organize themselves to create networks connecting fibroblasts together and to their environment [27,28], leading to tissue retraction *in vitro*. Lower extracellular matrix density is hen related to lower tissue retraction during maturation.

When it comes to the repartition of the human dermal microvascular endothelial cells within the tissue, clear organization in connected cell networks was observed. Nevertheless the presence of endothelial cell spheroids was also indicative of poor cell viability (red arrows pointing spheroids in Supplementary information 3-C). Finally, when searching for the presence of lumen based microvascular organization within this large bioprinted tissue matured under static conditions, no such structure can be identified, suggesting an incomplete maturation of the endothelial cells' network.

4. Conclusions

As a result of such preliminary study, a clear conclusion is the strong impact of the dynamic culture on the possibility to generate and maintain millimeter size tubular structures within a dm^3 bioprinted tissue. Indeed, identical tissues showed significantly different evolutions of their internal geometry when submitted or not to a constant perfusion flow. This result is clearly related to the hydromechanical stress generated by the medium solution flowing within the millimeter size internal structure of the bioprinted object.

At the cellular level, though observation of extracellular matrix formation, the lower production of collagen within the bioprinted tissue cultured under static conditions clearly indicates a lower maturation rate of the tissue (collagen production by human fibroblasts). This is certainly related to a poor conservation of tissues internal porosity, leading to a hindered culture medium diffusion within the tissue. Then, by analyzing the human dermal microvascular endothelial cells' organization, a clear difference was observed between dynamic and static culture conditions. This difference was already recently observed in cellularized biomaterial scaffolds cultured under direct flow conditions [8]. Vessel network morphogenesis and extracellular matrix protein distribution were then clearly enhanced in the presence of the hydromechanical stress. The later led to less micro-structured network organization, with no lumen based microstructures and the presence of spheroids, typical of environmental stress of the cells [29,30]. This observation has to be linked to the lower ECM production within the large bioprinted tissue matured under static condition. It could also be related to the fact that the ECM impacts

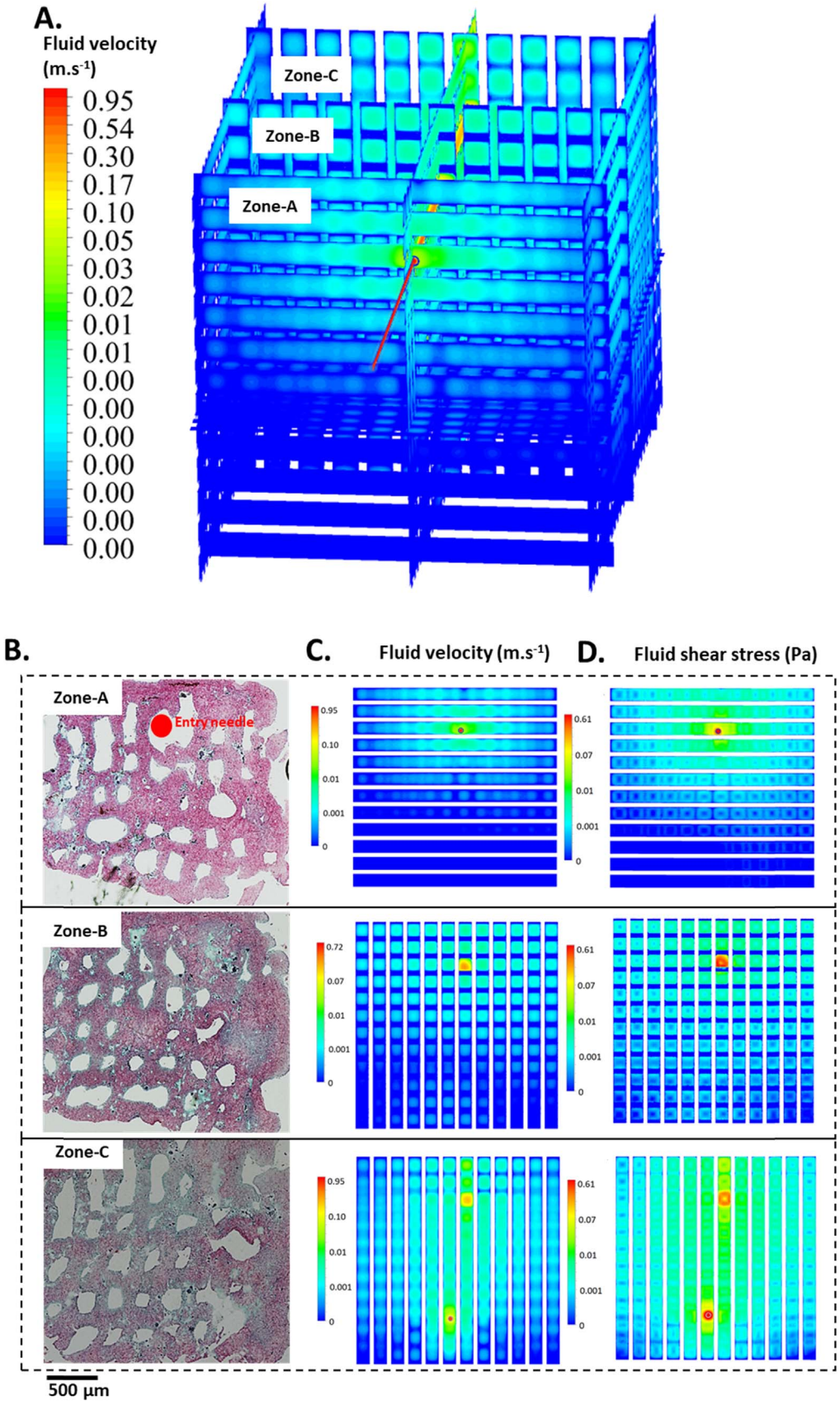

Fig. 2. A:Fluid flow velocity fields from CFD simulation of three different zones within the large bioprinted tissue. B:Characterization of 5 µm sections of the bioprinted large tissue after 12 days of dynamic culture. Full-size view of the large bioprinted tissue (Masson's Trichrome). C:Corresponding fluid flow velocity fields of zones A, B and C from CFD simulations. D:Corresponding fluid shear stress fields of zones A, B and C from CFD simulations.

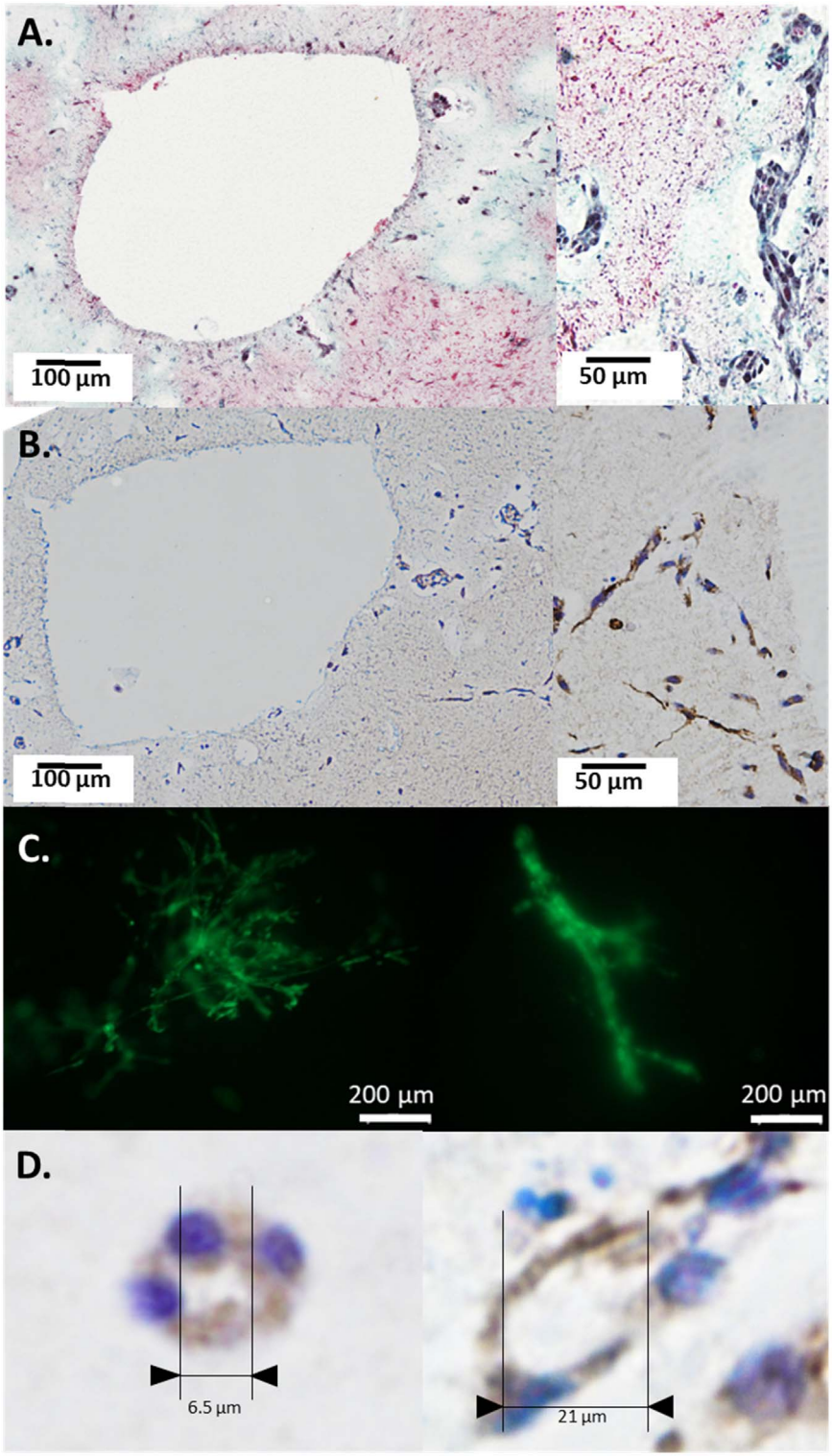

Fig. 3. Histological and immunohistological characterizations of 5 µm sections of the bioprinted large tissue after 7 days of dynamic culture. A: Masson's Trichrome staining of perfusion pore and a closer view of the surrounding tissue (violet staining of nuclei, green staining of collagen or ECM). B: EN4 immunohistochemistry staining (brown cytoplasmic staining) of the same perfusion pore and a closer view of the same surrounding tissue. C: Fluorescent microscopy images showing human dermal microvascular endothelial cells network. D: EN4 immunohistochemistry staining of human dermal microvascular endothelial cells organized around an open lumen.

directly the behavior of the embedded cells which might either, adhere and spread to form organized tissue structure, or regroup and form spheroids.

The results presented in this short study were meant to evaluate the impact of the concomitant use of an oriented internal millimeter size porosity and dynamic culture conditions (perfusion) on the maturation of a large bioprinted tissue (dm^3) incorporating cell components useful for micro-vascularization development (human dermal microvascular endothelial cells). The obtained results clearly indicate that the developed procedure enables, in one hand the conservation of the internal porosity of the bioprinted tissue, leading to a constant and homogeneous perfusion of the entire tissue, and in the other hand the

development of a clear organization in connected endothelial cell networks. Of course, numerous additional studies might now be performed to clarify whether or not the produced endothelial cell network can be matured toward a connection to the perfusion network, but these preliminary results are of great impact in the field since dm^3 vascularized bioprinted tissues maturation is expected to be next breakthrough in tissue engineering.

Acknowledgement

This work was supported by the French ANR (Agence Nationale de la Recherche) program ASTRID (project BLOC-PRINT - ANR-16-ASTR-0021), led and funded by the Direction Générale de l'Armement (DGA). The authors also sincerely thank Dr. Jean-Jacques Feige (CEA/DRF/BIG/BCI) for supplying human dermal microvascular endothelial cells (hDMEC) expressing GFP.

Appendix A. Supporting information

Supplementary data associated with this article can be found in the online version at doi:10.1016/j.bprint.2018.e00039.

References

[1] Y.J. Seol, et al., Bioprinting technology and its applications, Eur. J. Cardio-Thorac. Surg. 46 (3) (2014) 342–348.
[2] M. Gelinsky, A. Bernhardt, F. Milan, Bioreactors in tissue engineering: advances in stem cell culture and three-dimensional tissue constructs, Eng. Life Sci. 15 (7) (2015) 670–677.
[3] I. Martin, D. Wendt, M. Heberer, The role of bioreactors in tissue engineering, Trends Biotechnol. 22 (2) (2004) 80–86.
[4] L.E. Gallo-Ramirez, et al., Bioreactor concepts for cell culture-based viral vaccine production, Expert Rev. Vaccin. 14 (9) (2015) 1181–1195.
[5] V. Olivier, et al., In vitro culture of large bone substitutes in a new bioreactor: importance of the flow direction, Biomed. Mater. 2 (3) (2007) 174–180.
[6] R.F. Canadas, et al., Bioreactors and microfluidics for osteochondral interface maturation, Adv. Exp. Med. Biol. 1059 (2018) 395–420.
[7] I. Mannhardt, A. Marsano, A. Teuschl, Perfusion bioreactors for prevascularization strategies in cardiac tissue engineering, in: W. Holnthoner (Ed.)Vascularization for Tissue Engineering and Regenerative Medicine (2017), 2017.
[8] B. Zohar, et al., Flow-induced vascular network formation and maturation in three dimensional engineered tissue, ACS Biomater. Sci. Eng. 4 (4) (2018) 1265–1271.
[9] L.J. Pourchet, et al., Human skin 3D bioprinting using scaffold-free approach, Adv. Healthc. Mater. 6 (4) (2017).
[10] A. Desroches-Castan, et al., A new chemical inhibitor of angiogenesis and tumorigenesis that targets the VEGF signaling pathway upstream of Ras, Oncotarget 6 (7) (2015) 5382–5411.
[11] D.B. Kolesky, et al., Three-dimensional bioprinting of thick vascularized tissues, Proc. Natl. Acad. Sci. USA 113 (12) (2016) 3179–3184.
[12] L. Shahabeddin, et al., Characterization of skin reconstructed on a chitosan-cross-linked collagen-glycosaminoglycan matrix, Skin. Pharmacol. 3 (2) (1990) 107–114.
[13] J. Malda, et al., Oxygen gradients in tissue-engineered Pegt/Pbt cartilaginous constructs: measurement and modeling, Biotechnol. Bioeng. 86 (1) (2004) 9–18.
[14] J.C. Geesin, et al., Ascorbic acid specifically increases type I and type III procollagen messenger RNA levels in human skin fibroblasts, J. Investig. Dermatol. 90 (4) (1988) 420–424.
[15] R. Gauvin, et al., Minimal contraction for tissue-engineered skin substitutes when matured at the air–liquid interface, J. Tissue Eng. Regen. Med. 7 (6) (2013) 452–460.
[16] J.C. Wolchok, et al., The effect of bioreactor induced vibrational stimulation on extracellular matrix production from human derived fibroblasts, Biomaterials 30 (3) (2009) 327–335.
[17] R.E. Ayata, et al., Behaviour of endothelial cells in a tridimensional In vitro environment, BioMed. Res. Int. 2015 (2015) 9.
[18] I. Sukmana, P. Vermette, The effects of co-culture with fibroblasts and angiogenic growth factors on microvascular maturation and multi-cellular lumen formation in HUVEC-oriented polymer fibre constructs, Biomaterials 31 (19) (2010) 5091–5099.
[19] A. Armulik, A. Abramsson, C. Betsholtz, Endothelial/pericyte interactions, Circ. Res. 97 (6) (2005) 512–523.
[20] Z. Chen, et al., In vitro angiogenesis by human umbilical vein endothelial cells (HUVEC) induced by three-dimensional co-culture with glioblastoma cells, J. Neuro-Oncol. 92 (2) (2009) 121–128.
[21] X. Chen, et al., Prevascularization of a fibrin-based tissue construct accelerates the formation of functional anastomosis with host vasculature, Tissue Eng. Part A 15 (6) (2009) 1363–1371.
[22] W.H. Zhu, et al., The mouse aorta model: influence of genetic background and aging on bFGF- and VEGF-induced angiogenic sprouting, Angiogenesis 6 (3) (2003) 193–199.
[23] V. Nehls, K. Denzer, D. Drenckhahn, Pericyte involvement in capillary sprouting during angiogenesis in situ, Cell Tissue Res. 270 (3) (1992) 469–474.
[24] M.N. Nakatsu, et al., Angiogenic sprouting and capillary lumen formation modeled by human umbilical vein endothelial cells (HUVEC) in fibrin gels: the role of fibroblasts and Angiopoietin-1, Microvasc. Res. 66 (2) (2003) 102–112.
[25] O.C. Velazquez, et al., Fibroblast-dependent differentiation of human microvascular endothelial cells into capillary-like 3-dimensional networks, FASEB J.: Off. Publ. Fed. Am. Soc. Exp. Biol. 16 (10) (2002) 1316–1318.
[26] V. Lee, et al., Design and fabrication of human skin by three-dimensional bioprinting, Tissue Eng. Part C Methods 20 (6) (2014) 473–484.
[27] P.A.J. Kolarsick, M.A. Kolarsick, C. Goodwin, Anatomy and physiology of the skin, J. Dermatol. Nurses' Assoc. 3 (4) (2011) 203–213.
[28] V. Marcos-Garcés, et al., Age-related dermal collagen changes during development, maturation and ageing – a morphometric and comparative study, J. Anat. 225 (1) (2014) 98–108.
[29] T.-C. Tseng, et al., Biomaterial substrate-mediated multicellular spheroid formation and their applications in tissue engineering, Biotechnol. J. 12 (12) (2017) (p. 1700064-n/a).
[30] X.Z. Shu, et al., Attachment and spreading of fibroblasts on an RGD peptide-modified injectable hyaluronan hydrogel, J. Biomed. Mater. Res. Part A 68A (2) (2004) 365–375.